ChemistrySelect

Research Article
doi.org/10.1002/slct.202404272

Chemistry Europe
European Chemical Societies Publishing

www.chemistryselect.org

Fabrication and Characterization of Calcium Alginate Beads with a Specially Designed Magnetic Pulse Encapsulator

Seyda Demircan,[a] Huseyin Demircan,[a] Kemal Sarioglu,[b] Ergun Ates,[c] Nadide Seyhun,[a] and Rasim Alper Oral*[a]

In this study, a novel encapsulator system based on magnetic field principles was developed to produce gallic acid-loaded beads with an adjustable particle size and high production capacity. A dripping device was designed and optimized using the response surface methodology with a central composite design. Alginate concentration, nozzle diameter, frequency, distance, and flow rate were selected as independent variables. Bead properties, including encapsulation efficiency, production yield, loading capacity, particle diameter, aspect ratio, circularity, sphericity, polydispersity index, span, D10, D50, and D90, values were evaluated as response variables. In vitro release kinetics of the beads were investigated. Particle shape was mainly affected by all parameters except flow rate, while size distribution was predominantly governed by the alginate concentration, nozzle diameter, and frequency. Bead morphology strongly affected the release behavior, with smaller and more spherical beads showing faster release rates. The developed system successfully produced small-sized beads with high encapsulation efficiency (up to 60.7%). These findings demonstrate the potential of the proposed magnetic encapsulation system for the efficient encapsulation of gallic acid and other water-soluble phenolic compounds. Furthermore, its adaptability to multi- or interchangeable nozzle configurations makes it suitable for pilot- or industrial-scale production.

1. Introduction

Gallic acid, a.k.a. 3,4,5-trihydroxybenzoic acid ($C_7H_6O_5$), is a well-known reference standard material for food analysis. It is a critical phenolic compound present in grapes, cereals, berries, black tea, nuts, herbs, and in the leaves of many plants.[1–3] Apart from being a certified reference material, gallic acid is also known for its numerous physiological and biochemical properties, such as antioxidant, antimicrobial, anti-aging, anti-inflammatory, anti-carcinogenic, cardiovascular protective, and gastroprotective activities.[2–5] Although it has a promising potential for functional food applications, its bitterness and astringency limit the use of gallic acid. In addition, it is unstable at extreme temperatures or in the presence of light and oxygen and tends to auto-oxidize.[1,3,4] Therefore, encapsulation is a suitable way of delivery for gallic acid to enhance its storage stability.

Encapsulation is a successful method for transporting bioactive molecules (antioxidants, minerals, vitamins, phytosterols, lutein, fatty acids, lycopene, etc.) and living cells (probiotics, etc.) in foods. It is a technology in which the active material is covered or trapped within another material, where the contents of the bead can be released in a controlled manner under particular conditions.[6–8] While the active material could be called the core material, filling, or internal phase, the wall material could be called the shell, carrier material, coating material, membrane, or external phase.[9,10]

The first use of encapsulation technology and bead preparation dates back to the 1950s. Technologies developed for carbonless copy paper led to the development of various bead products in the following years.[11] Today, fields such as food, agriculture, biotechnology, chemistry, textiles, feed, medicine, cosmetics, and veterinary are examples of sectors where encapsulation is considerably used.[12] Microencapsulation finds its place in food technology for purposes such as increasing the shelf life of foods, improving product quality, stabilizing an active ingredient, masking the unpleasant taste of bioactive compounds, and ensuring the controlled release of these substances.[13,14]

There is no universal approach for encapsulation. Different encapsulation techniques can be used according to the active and wall materials. The encapsulation techniques vary depending on the bioactive material, the carrier food, and the physical and chemical properties of the release mechanism of the active material.[15,16] These techniques are grouped under three headings: physical, chemical, and physicochemical techniques.[17] There are various techniques for the encapsulation of food ingredients in the literature. Methods such as ionic gelation, spray drying, fluidized bed coating, emulsion, extrusion, coacervation, liposome coating, co-crystallization, and the pH-driven method can be used for numerous purposes.[18–20] Extrusion techniques can be applied electrostatically with coaxial airflow, with vibrating nozzles and rotating atomizer discs. The technique of encapsulation by extrusion with vibratory technology is effective and reproducible for the preservation and

[a] S. Demircan, Asst. Prof. H. Demircan, Asst. Prof. N. Seyhun, Prof. R. A. Oral
Department of Food Engineering, Faculty of Engineering and Natural Sciences, Bursa Technical University, Bursa 16310, Türkiye
E-mail: rasim.oral@btu.edu.tr

[b] Prof. K. Sarioglu
Department of Food Engineering, Faculty of Engineering, Erciyes University, Kayseri 38039, Türkiye

[c] Prof. E. Ates
Department of Mechanical Engineering, Faculty of Engineering, Balıkesir University, Balıkesir 10145, Türkiye

stability of bioactive ingredients. Beads are obtained by mixing the droplets formed with the encapsulating material after the core material is passed through an injector nozzle that applies a certain vibration frequency. It has been reported that this vibration can be achieved by the simultaneous entry of the feed and air into the nozzle.[21]

Ionic gelation is a promising encapsulation technique because it does not require high temperature, vigorous mixing, or organic solvents.[22,23] It is an easy and efficient way of encapsulation and can be considered cost-effective.[22,24] In this direction, the importance of an encapsulator device and encapsulation system with low cost, capacity, and features suitable for industrial production is increasing. The volumes of bead production made on a laboratory scale with syringe pumps are low and unsuitable for industrial production. The studies in the literature on bead production using ionic gelation show that the bead production rates are in the range of 0.17–2.00 mL/min.[13,24,25] With these production rates, a maximum of 1.2 L alginate-core material solution encapsulation can be realized during 10 h of production.

Compared to traditional encapsulation methods like electrospray and emulsion techniques, the magnetic encapsulation strategy developed in this study provides an innovative mechanism for improving droplet control and production efficiency. Electrospray systems can produce fine particle sizes; nevertheless, they generally require high voltages and yield poor production capacity, hence constraining their scalability for industrial applications.[26,27] Emulsion-based approaches, meanwhile, entail intricate multi-phase systems and frequently necessitate surfactants or organic solvents, which may raise biocompatibility issues and impede particle size uniformity.[28,29] This paper presents a magnetic-assisted encapsulator system that uses the ionic gelation of alginate-calcium droplets, incorporating a magnetically responsive needle that oscillates due to attraction and repulsion near a revolving magnetic shaft. This dynamic contact facilitates the production of markedly smaller droplets with enhanced homogeneity and increased production capacity relative to the traditional dripping techniques. Consequently, this system provides a simple, clean, scalable, and efficient substitute for conventional encapsulation methods.

The objective of this study is to suggest a novel encapsulation method that enables the different-sized beads by using a magnetic vibration mechanism to increase the production capacity and the encapsulation efficiency of gallic acid in calcium alginate beads. Due to the working principle of the designed encapsulation system, it was aimed to reduce the produced bead size and increase production capacity with the help of oscillating nozzle breaking of the surface tension of the droplets early. In this context, the encapsulation process was carried out using the ionic gelation method based on the principle of the cross-linking of calcium and alginate. Different alginate concentrations (1%, 2%, and 3%), nozzle diameters (0.514, 0.676, and 0.838 mm), frequencies (500, 750, and 1000 rpm), distances (40, 50, and 60 mm), and flow rates (1.0, 4.5, and 8.0 mL/min) were used for the bead production. The encapsulation efficiency, production yield, loading capacity, particle diameter, aspect ratio, circularity, sphericity, polydispersity index, D10 value, D50 value, D90 value, and span factor values of the obtained beads were analyzed.

2. Materials and Methods

2.1. Materials

The gallic acid, calcium chloride dihydrate ($CaCl_2.2H_2O$), and sodium alginate used in this study were obtained from Sigma–Aldrich (USA). The encapsulator used for encapsulation was specially designed and produced on a lathe.

2.2. Encapsulation

2.2.1. Encapsulator Design

The 3D drawing of the designed magnetic apparatus system is shown in Figure 1. According to the designed system, the alginate-core material (i.e., gallic acid) mixture solution is fed to the nozzle to drop into the calcium chloride bath with a syringe pump (Goldman/AR-03). Syringe needles with different inner diameters were used as the nozzles. The needle was mounted to the apparatus system with a flexible metal rod, and a 20 × 10 mm circular neodymium magnet was placed on the other end of the rod. A 30 × 30 × 30 mm cube-shaped neodymium magnet was attached to the end of a stainless steel rod, and this rod was placed in a mechanical stirrer. Neodymium magnets were specifically selected due to their exceptionally high magnetic strength, which enables effective transmission of the magnetic force across relatively large distances and allows for precise control of the needle movement within the system.

2.2.2. Bead Production

The encapsulation process was carried out by the ionic gelation method. Gallic acid, a phenolic compound, was used as the active material. After the gallic acid solution (0.5% w/v) was prepared, different amounts of sodium alginate (1%, 2%, and 3% w/v) were added to the gallic acid solution as the wall material and mixed homogeneously with a mechanical mixer (Heidolph/Hei-TORQUE Value 100). The wall and active material mixture (10 mL) was fed with a syringe pump (Goldman/AR-03) with different flow rates into a 2% (w/v) calcium chloride ($CaCl_2$) solution containing 0.5% (w/v) gallic acid. Three different needles with three different inner diameter values (0.514 mm (21G), 0.676 mm (19G), and 0.838 mm (18G)) were used as the nozzle. The encapsulation process was carried out by dripping at different speeds (1.0, 4.5, and 8.0 mL/min).[15] The gap between the magnet on the main shaft and the magnet attached to the needle was set to different distances of 40, 50, and 60 mm. The main shaft worked at frequency values of 500, 750, and 1000 rpm. The system was mixed with a magnetic stirrer during the dripping process to prevent the aggregation of dripping solutions before the gelation was complete. The beads were mixed for 30 min. to complete the hardening. Then, the beads were filtered with a strainer and washed with approximately 150 mL of distilled water

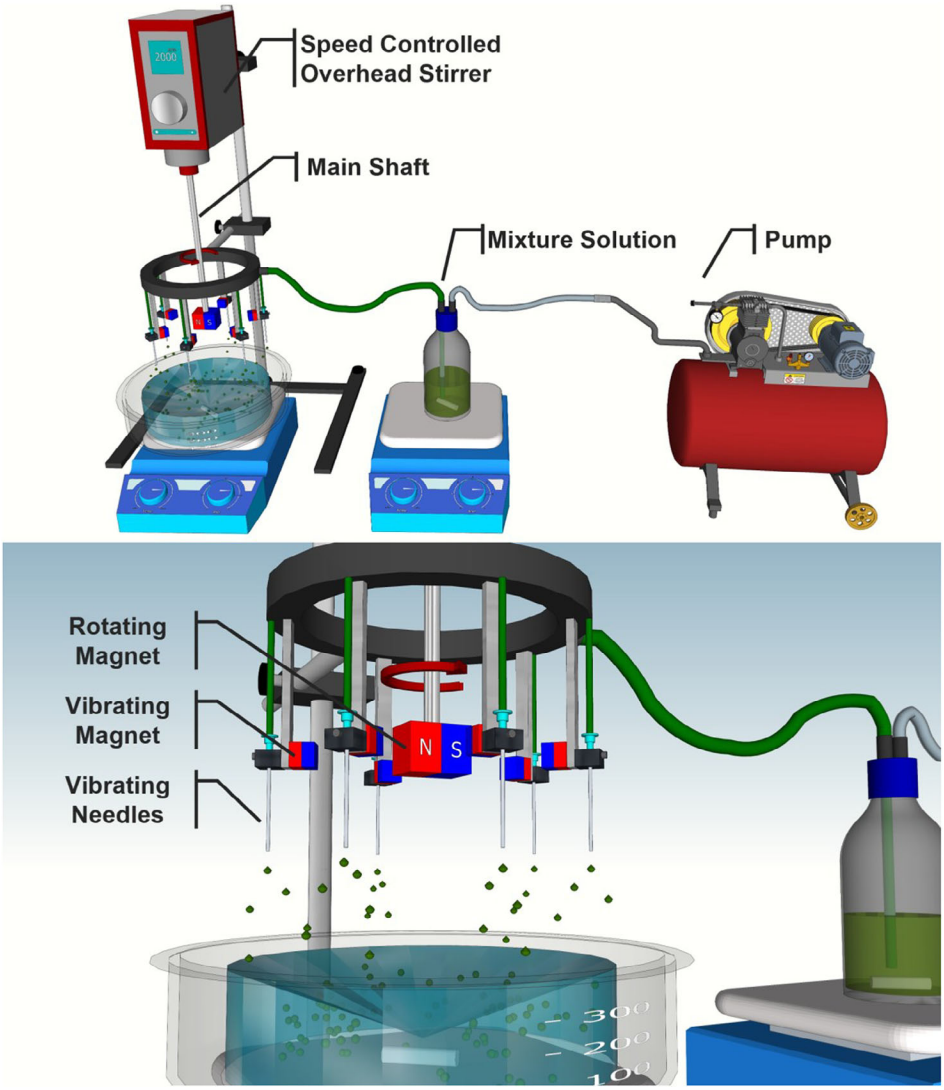

Figure 1. Designed magnetic pulse encapsulator system.

to remove the ungelled calcium from their surfaces. They were then dried in a fume hood at room condition for 24 h.[24] The dried beads were weighed, placed into capped glass bottles, and stored at room temperature for further analysis.

2.3. Bead Analyses

2.3.1. Particle Size and Shape by Image Analysis

The beads were produced for each experiment in the model design. Images of 20 randomly selected beads were taken from the dry particles obtained from these productions using a Leica EZ4-E stereo zoom microscope. The obtained bead images were processed using ImageJ 1.53f51v software (USA), and the particle diameter (PD), aspect ratio (AR), and circularity values were recorded. The sphericity factor (Φ) was calculated using Equation (1).[30,31]

$$\Phi = \frac{2D_{min}}{D_{min} + D_{max}} \times 100 \quad (1)$$

In Equation (1), D_{min} represents the minimum diameter of the particle, and D_{max} represents the maximum diameter. The polydispersity index (PDI), which shows the size distribution of the particles, was calculated using Equation (2).[32]

$$PDI = \frac{D_{SD}{}^2}{D_{Ave}{}^2} \quad (2)$$

The D_{SD} value in Equation (2) represents the standard deviation of the particle diameter, and the D_{Ave} value represents the mean particle diameter. The span factor was calculated using Equation (3).[33]

$$Span = \frac{D_{90} - D_{10}}{D_{50}} \quad (3)$$

The D10, D50, and D90 values in Equation (3) represent the particle diameters at which 10%, 50%, and 90% of the total particle population are smaller than the given value, respectively. Specifically, D10 represents the size below which 10% of the particles fall, D50 is the median particle size, and D90 indicates the size below which 90% of the particles are found. These val-

ues provide insight into the overall particle size distribution and spread.

2.3.2. Encapsulation Efficiency, Production Yield, and Loading Capacity

Twenty mg of the obtained beads were weighed and placed into a beaker. After adding 40 mL of distilled water, the beads were crushed using a homogenizer (VelpScientifica/OV5) at 10,000 rpm for 2 min. Then, sonication was carried out in an ultrasonic water bath (Daihan-WiseClean/WUC-D10H) at 300 W power for 2 min. The solution in the beaker was passed through a 0.45 µm syringe filter and transferred to vials for HPLC analysis.[34] An HPLC (Agilent/Infinity 1260) device was used to analyze the gallic acid content of the beads. A C18 column (150 × 4.6 mm, 5 µm) and a DAD detector were used. The flow rate was determined as 1 mL/min, the column temperature was 25 °C, and the wavelength was 280 nm. Ultrapure water with 1:1 acetic acid and methanol was used as the mobile phase. The isocratic elution program was applied, and the analysis time was determined to as 5 min. The obtained peaks were evaluated with the gallic acid standard graph (0–100 ppm).

The encapsulation efficiency (EE), production yield (PY), and loading capacity (LC) of the produced beads were calculated according to Equations (4–6), respectively.

$$EE\ (\%) = \frac{M_{ga1}}{M_{ga0}} \times 100 \quad (4)$$

$$PY\ (\%) = \frac{M_p}{M_t} \times 100 \quad (5)$$

$$LC\ (\%) = \frac{M_{ga1}}{M_p} \times 100 \quad (6)$$

M_p: weight of the beads produced (g), M_t: weight of the wall and core material used (g), M_{ga0}: the amount of gallic acid used in encapsulation (g), M_{ga1}: the amount of gallic acid in the bead (g).

2.4. Experimental Design and Statistical Analysis

The obtained data were evaluated using the Design Expert v12 program, and the effects of the experimental parameters on the dependent variables were expressed as a model equation. The factors chosen for the model were carefully selected to reflect the most influential variables in the encapsulation process, including the sodium alginate concentration, nozzle diameter, frequency, distance between the rotating and vibrating magnets, and flow rate. The independent variables and coded levels used in the experimental design are given in Table 1. Nozzle diameter in Table 1 refers to syringe needles with different inside diameter values, frequency refers to the number of revolutions per minute of the mechanical mixer, and distance refers to the distance between the magnet at the end of the main shaft of the mechanical stirrer and the magnet mounted on the needle. Primarily, a two-level factorial design with three center points was performed to determine the effects of the parameters (Table 2, first 19 runs). Since the model curvature of the factorial design was significant, indicating that the model was nonlinear, additional test points (runs between 20 and 31) were added to the experimental design (Table 2), and the Response Surface Method/Central Composite Design (RSM-CCD) was carried out. In the realized central composite design, five central points were used. The encapsulation efficiency (EE), production yield (PY), loading capacity (LC), particle diameter (PD), aspect ratio (AR), circularity, sphericity, polydispersity index (PDI), span factor, D10, D50, and D90 values were determined as dependent variables (responses). Analysis of variance (ANOVA) was performed for each dependent variable. The most suitable model was selected according to the model p-value, the lack of fit p-value, R^2, adjusted R^2, and predicted R^2 values.

Table 1. Coded levels of independent variables used in bead production.

Independent Variables	Unit	Code	Coded Levels		
			−1	0	+1
Alginate concentration	%	X_1	1.0	2.0	3.0
Nozzle diameter	mm	X_2	0.514	0.676	0.838
Frequency	rpm	X_3	500	750	1000
Distance	mm	X_4	40	50	60
Flow rate	mL/min	X_5	1.0	4.5	8.0

2.5. In Vitro Release Kinetics

In the controlled release analysis, beads obtained from three different productions were used, where all of the independent variables used in bead production were minimum (R14), average (R15), and maximum (R8). Release analysis was carried out by modifying the methods of Kiaei Pour et al. (2020) and Vaziri et al. (2019).[35,36] Simulated gastric juice (SGJ) consisted of 1.0 g sodium chloride (NaCl) and 1.6 g pepsin (0.7 FIP-U/mg) in 3.5 mL hydrochloric acid (HCl, 37%) and diluted to 500 mL with distilled water. The pH of SGJ was adjusted to 2.0 with 0.2 N sodium hydroxide (NaOH) solution. Simulated intestinal juice (SIJ) consisted of 3.4 g potassium dihydrogen phosphate (KH_2PO_4), 5.0 g pancreatin, and 2.5 g bile salt in distilled water. The pH of the solution was adjusted to 7.5 ± 0.1 with 0.2 N NaOH and diluted to 500 mL with distilled water. In the release behavior analysis, 75 mg of dried beads were transferred into a Falcon tube containing 40 mL of SGJ at 37 °C. The mixture was incubated at 37 °C with shaking at 100 rpm for 2 h. Samples were taken at the 5, 10, 15, 30, 60, 90, and 120th min to be used in the HPLC gallic acid content analysis. Then, the beads were filtered and washed with distilled water to neutralize the pH and transferred into another tube containing 40 mL of SIJ at 37 °C. Incubation was repeated under the same conditions for 2 h. Samples were taken at every 30 min time interval, and HPLC gallic acid content

Table 2. Coded levels of response surface methodology–Central Composite Design (RSM-CCD).

	Independent Variables				
Run	Alginate Concentration (%)	Nozzle Diameter (mm)	Frequency (rpm)	Distance (mm)	Flow Rate (mL/min)
1	+1	−1	+1	+1	−1
2	−1	−1	−1	+1	−1
3	+1	+1	−1	+1	−1
4	+1	−1	−1	+1	+1
5	+1	−1	−1	−1	−1
6	−1	+1	+1	+1	−1
7	+1	+1	+1	−1	−1
8	+1	+1	+1	+1	+1
9	0	0	0	0	0
10	−1	+1	−1	+1	+1
11	+1	+1	−1	−1	+1
12	0	0	0	0	0
13	+1	−1	+1	−1	+1
14	−1	−1	−1	−1	+1
15	0	0	0	0	0
16	−1	−1	+1	−1	−1
17	−1	−1	+1	+1	+1
18	−1	+1	−1	−1	−1
19	−1	+1	+1	−1	+1
20	0	0	+1	0	0
21	+1	0	0	0	0
22	0	0	0	0	0
23	0	+1	0	0	0
24	0	0	0	0	−1
25	0	0	0	−1	0
26	0	0	0	+1	0
27	0	−1	0	0	0
28	−1	0	0	0	0
29	0	0	−1	0	0
30	0	0	0	0	0
31	0	0	0	0	+1

analysis was performed. The cumulative gallic acid release of the beads was measured as a function of time. Exponential and hyperbolic equations were used in the modeling of the gallic acid release kinetics (Equations 7 and 8).[37,38]

Exponential equation.

$$\text{Cumulative gallic acid release } (\%) = a \times \left(1 - e^{(-b \times t)}\right) \quad (7)$$

Hyperbolic equation.

$$\text{Cumulative gallic acid release } (\%) = \frac{(a \times t)}{(b + t)} \quad (8)$$

a and b: the model coefficients, t: time (min).

3. Results and Discussion

3.1. Bead Production and Model Evaluation

In this study, alginate bead production was carried out using a newly developed magnetic pulse encapsulator system, as shown in Figure 1. This system provides simple, clean, scalable, and efficient bead production. One of the main disadvantages of calcium alginate bead production is the limitations in scale-up potential. Notably, the throughput of such extrusion systems has been reported to vary between approximately 10 and 360 mL/h, which implies that scaling up production to meet industrial demands could require either extensive parallelization or significant process redesign.[39] Preliminary trials have shown that by using the developed apparatus at full capacity, a production capacity increase of more than five times can easily be achieved

Research Article
doi.org/10.1002/slct.202404272
Chemistry Europe
European Chemical Societies Publishing

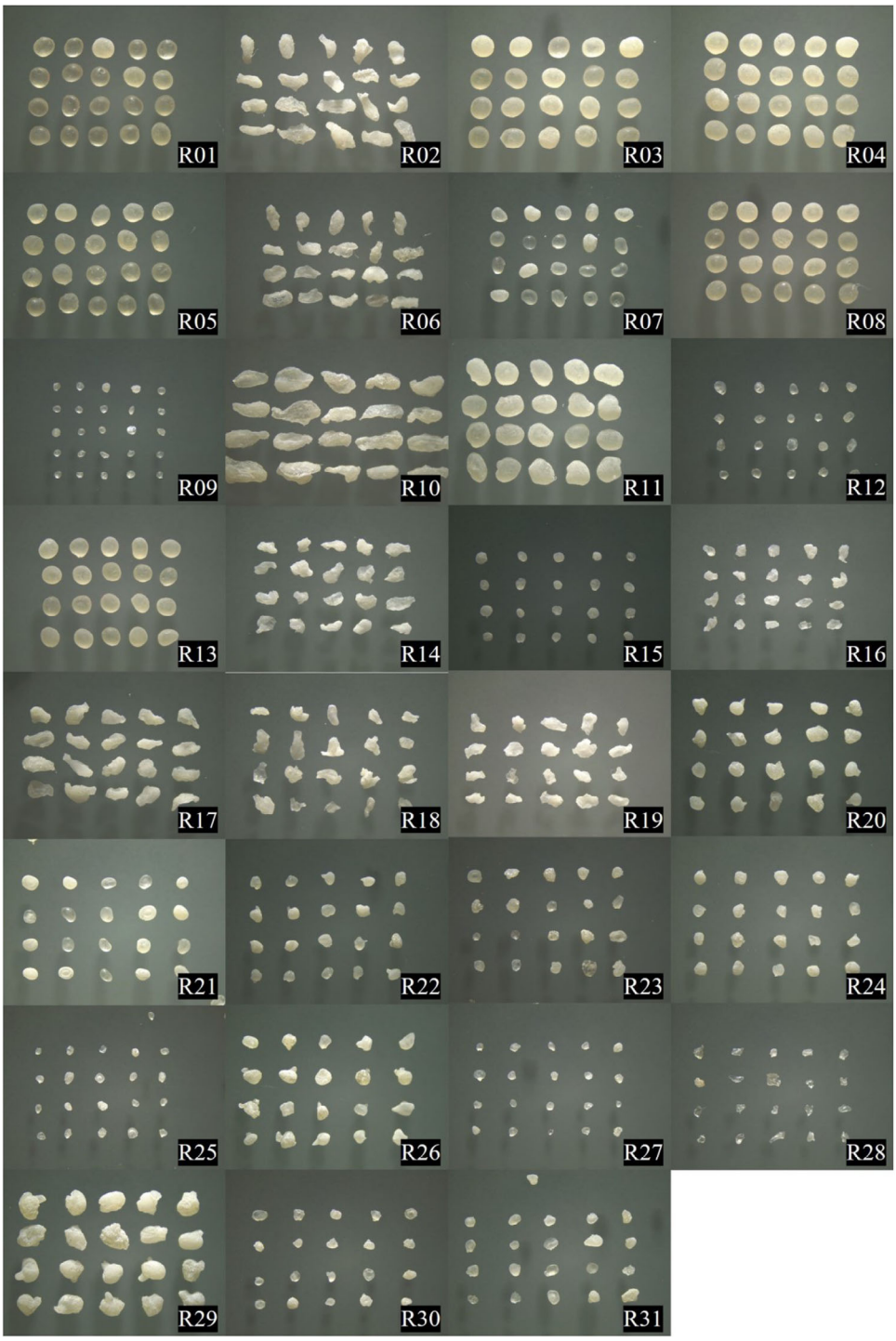

Figure 2. Microscope images of the produced beads (8x).

compared to production with a traditional syringe pump. With this increase, the large-scale production of calcium alginate beads can be more readily achieved. Such scalability enhances the practical applicability of the method for various sectors, including pharmaceuticals, nutraceuticals, and functional food industries, where efficient and consistent encapsulation is critical.

The microscope images (8x) of 31 beads produced according to the parameters determined in RSM-CCD are given in Figure 2. EE, PY, LC, PD, AR, circularity, sphericity, PDI, D10, D50, D90, and span properties were examined, and the results are shown in Table 3. The ANOVA table *F*-values and reduced quadratic model equations of all responses are given in Tables 4 and 5, respectively. Diagnostic evaluation of the quadratic models confirmed their suitability. Normal probability plots revealed that the standardized residuals followed a trend that was close to linear. On the other hand, "predicted versus actual" and "residuals versus predicted" plots showed random scatter without curva-

Table 3. Bead production experimental design results.

Run	EE (%)	PY (%)	LC (%)	PD (mm)	AR	Circularity	Sphericity	PDI	D10 (mm)	D50 (mm)	D90 (mm)	Span
1	45.6	134.7	4.84	1.173	1.12	0.894	94.5	0.0011	1.131	1.161	1.239	0.0929
2	26.4	142.2	6.19	1.197	2.21	0.620	63.8	0.0148	1.004	1.175	1.457	0.3854
3	60.7	150.6	5.75	1.277	1.15	0.893	93.2	0.0003	1.260	1.273	1.309	0.0387
4	57.7	150.4	5.49	1.293	1.12	0.893	94.6	0.0013	1.258	1.295	1.339	0.0624
5	58.7	146.7	5.71	1.166	1.12	0.891	94.5	0.0005	1.127	1.166	1.196	0.0596
6	23.5	125.1	6.26	1.056	2.06	0.647	66.2	0.0138	0.909	1.052	1.235	0.3100
7	52.0	142.1	5.22	0.898	1.27	0.875	88.4	0.0019	0.856	0.892	0.954	0.1103
8	59.8	150.5	5.67	1.179	1.15	0.890	93.0	0.0008	1.137	1.176	1.221	0.0719
9	25.1	106.7	4.71	0.434	1.21	0.886	90.9	0.0082	0.385	0.427	0.498	0.2660
10	34.1	164.5	6.90	1.554	2.30	0.614	61.6	0.0184	1.345	1.498	1.870	0.3503
11	60.4	158.6	5.44	1.453	1.27	0.857	88.7	0.0010	1.416	1.452	1.497	0.0553
12	26.8	110.1	4.88	0.575	1.24	0.865	89.6	0.0124	0.504	0.558	0.642	0.2462
13	54.0	141.5	5.45	1.110	1.15	0.892	93.3	0.0006	1.074	1.114	1.141	0.0607
14	21.4	129.4	5.52	0.946	1.69	0.683	76.2	0.0137	0.804	0.923	1.066	0.2837
15	33.4	121.0	5.52	0.577	1.19	0.886	91.7	0.0111	0.507	0.566	0.668	0.2840
16	16.7	106.4	5.22	0.675	1.56	0.729	79.2	0.0118	0.592	0.670	0.769	0.2645
17	24.9	136.9	6.05	1.163	1.92	0.681	69.7	0.0096	1.031	1.144	1.326	0.2587
18	18.9	112.2	5.62	0.914	1.71	0.650	76.2	0.0333	0.701	0.917	1.132	0.4707
19	22.2	126.7	5.83	0.891	1.76	0.688	73.8	0.0177	0.747	0.884	1.034	0.3248
20	44.9	159.1	5.65	0.894	1.26	0.782	89.1	0.0078	0.806	0.886	1.042	0.2669
21	42.2	133.3	4.52	0.821	1.25	0.883	89.0	0.0059	0.741	0.820	0.894	0.1865
22	37.1	140.0	5.30	0.730	1.23	0.811	89.8	0.0033	0.677	0.723	0.791	0.1577
23	36.8	135.0	5.46	0.689	1.24	0.844	89.8	0.0284	0.528	0.675	0.851	0.4785
24	40.6	149.2	5.45	0.729	1.19	0.844	91.5	0.0050	0.665	0.735	0.801	0.1847
25	28.1	118.6	4.75	0.469	1.28	0.876	88.1	0.0164	0.408	0.448	0.568	0.3584
26	46.6	166.9	5.59	0.845	1.28	0.800	88.2	0.0083	0.730	0.831	0.945	0.2586
27	35.5	131.0	5.43	0.457	1.23	0.872	89.8	0.0235	0.367	0.448	0.540	0.3863
28	13.0	86.4	5.03	0.525	1.58	0.710	79.4	0.0252	0.447	0.514	0.614	0.3233
29	55.0	186.4	5.90	1.330	1.33	0.796	86.2	0.0047	1.202	1.331	1.407	0.1545
30	36.6	133.6	5.48	0.607	1.20	0.849	91.3	0.0135	0.512	0.598	0.700	0.3159
31	38.3	138.2	5.54	0.675	1.28	0.845	88.3	0.0181	0.573	0.658	0.786	0.3246

ture, which meant that the fit was good and the data was homoscedastic. Time sequence checks showed that there was no systematic drift. We also looked at influence diagnostics like Cook's distance, leverage, DFFITS, and DFBETAS. We removed any observations that were outside of the permitted ranges in these diagnostic plots and rebuilt the model accordingly. In general, these tests show that the quadratic models are good enough and work well. When the ANOVA results in Table 4 are examined, it is observed that the reduced quadratic models of all responses are statistically significant ($p < 0.001$). In addition, the lack of fit was statistically insignificant for all models ($p > 0.05$). Table 5 shows that the predicted R^2 values are in reasonable agreement with the adjusted R^2 values for all responses. The difference between these two values is required to be less than 0.2. In addition, it was determined that the adequate precision values were desirably greater than 4 for all response models. Except for the PDI and span values, the coefficient of variation (CV) values of all responses were found to be below approximately 10%, indicating good model reliability and reproducibility. The relatively higher CV values observed for PDI and span may be attributed to the small number of replicates and are likely to decrease with more measurements. The correlation values between all responses are given in Figure 3.

3.2. Encapsulation Efficiency (EE)

It was determined that the EE results varied between 13.00% and 60.70% (Table 3). As seen in Table 4, the alginate concentration, frequency, distance, and alginate concentration/distance interaction were effective on EE. Alginate concentration and frequency stand out as the two parameters with the most significant effect on EE ($p < 0.001$). The reduced quadratic model R^2, adjusted R^2, and predicted R^2 values for EE were found to be 0.9586, 0.9399, and 0.9055, respectively (Table 5). Thus, 90.55% of the EE value can be explained with the reduced quadratic model specified

Table 4. ANOVA table *F*-values for the reduced quadratic model of each dependent variable.

Source	EE	PY	LC	PD	AR	Circularity	Sphericity	PDI	D10	D50	D90	Span
Model	51.43[c]	13.90[c]	10.42[c]	31.26[c]	112.79[c]	108.71[c]	109.39[c]	20.79[c]	30.21[c]	30.38[c]	30.78[c]	20.37[c]
X_1	365.55[c]	10.59[b]	20.87[c]	17.08[c]	860.40[c]	714.74[c]	603.47[c]	85.91[c]	38.37[c]	16.13[c]	0.52	95.12[c]
X_2	3.24	–	5.18[a]	4.36	13.31[b]	7.25[a]	10.76[b]	2.39	1.72	3.38	6.79[a]	2.42
X_3	10.81[b]	8.71[b]	5.55[a]	35.68[c]	8.55[b]	6.14[a]	2.64	0.37	22.06[c]	27.45[c]	34.10[c]	0.97
X_4	9.58[b]	12.26[b]	16.06[c]	40.02[c]	49.10[c]	8.25[b]	20.03[c]	–	28.40[c]	29.85[c]	42.70[c]	–
X_5	3.81	4.79[a]	2.69	11.33[b]	1.32	–	–	–	8.52[b]	7.94[a]	9.02[b]	–
X_1X_3	–	–	–	–	10.16[b]	5.48[a]	3.37	–	–	–	–	4.38[a]
X_1X_4	4.66[a]	6.60[a]	12.35[b]	14.30[b]	101.65[c]	12.42[b]	59.41[c]	–	9.47[b]	10.44[b]	17.68[c]	–
X_2X_3	–	–	–	4.39[a]	–	–	–	–	3.70	3.23	4.39[a]	–
X_2X_4	–	–	3.70	–	–	–	–	–	–	–	–	–
X_2X_5	–	–	–	3.67	4.15	–	–	–	–	–	4.40[a]	–
X_3X_4	–	–	–	–	5.04[a]	–	–	–	–	–	–	–
X_1^2	12.74[b]	–	7.07[a]	–	145.24[c]	23.65[c]	66.05[c]	–	–	–	–	–
X_2^2	–	–	–	–	–	–	–	7.71[a]	–	–	–	15.63[c]
X_3^2	44.49[c]	41.32[c]	19.15[c]	109.31[c]	–	31.60[c]	–	14.39[c]	129.47[c]	144.66[c]	157.39[c]	18.43[c]
X_5^2	3.45	–	5.86[a]	3.20	–	–	–	–	–	–	–	–
Lack of fit	1.00	2.19	0.32	0.97	4.09	0.84	3.14	0.71	1.10	1.32	1.30	0.60

X_1: Alginate concentration, X_2: nozzle diameter, X_3: frequency, X_4: distance, and X_5: flow rate.
[a] $p < 0.05$.
[b] $p < 0.01$.
[c] $p < 0.001$.

in the table. A high correlation ($r = 0.9791$) was found between the predicted and actual EE values. It was observed that the EE values increased with the increase in the alginate concentration.

The concentration of sodium alginate is crucial in influencing the encapsulation efficiency (EE) and the handling characteristics of the polymer solution. Increasing the alginate content often elevates the viscosity and cross-link density of the gel matrix, thereby enhancing the trapping of active chemicals; nevertheless, a practical upper limit exists beyond which the solution becomes challenging to handle. Consistent with the findings of Wani and Uppaluri (2023), which indicated that highly viscous alginate solutions obstruct smooth flow through stainless steel needles during bead formation, our study similarly noted that elevated alginate concentrations resulted in operational difficulties and diminished the feasibility of bead production.[40] Similar observations were made by Wani and Uppaluri (2023), who highlighted that although higher alginate concentrations initially improve encapsulation efficiency, overly viscous solutions compromise the processing feasibility due to pumping limitations.[40] In another study, Borah et al. (2024) reported that a lower sodium alginate (SA) concentration led to insufficient solution viscosity and reduced cross-linking efficiency with Ca^{2+} ions, resulting in poor bead integrity and decreased encapsulation efficiency.[41] In a related study, Najafi-Soulari et al. (2016) also demonstrated that increasing the sodium alginate concentration led to higher encapsulation efficiency due to the formation of a thicker gel network, which limited the diffusion of the encapsulated compounds into the surrounding medium.[42] In another study, Gholamian et al. (2021) investigated the encapsulation of cumin seed essential oil in calcium alginate hydrogel beads and found that increasing the sodium alginate concentration enhanced the encapsulation efficiency and structural integrity of the beads.[43] This finding aligns with our hypothesis that higher alginate concentrations lead to a stronger gel matrix, thereby improving the encapsulation efficiency.

On the other hand, the EE values decreased at the 750 rpm frequency and increased again with the increase in frequency. When the correlation table between the dependent variables was examined (Figure 3), a high positive correlation of 0.94, 0.93, 0.94, and 0.93 was found between the EE value and the PD, D10, D50, and D90 values, respectively. This shows that the particle size significantly affects the EE value. Since large particles have a relatively small surface area compared with small particles for the same mass, it is thought that the amount of core material diffused from the bead surface decreases, and therefore the EE value increases. Gouin (2004) stated that alginate beads have a porous structure, which causes the core material to diffuse easily out of the bead in the liquid matrix.[44]

Gallic acid, used as the core material, is a hydrophilic compound. Due to the porous structure of the alginate beads, it could be explained that gallic acid diffuses through the pores of the bead into the bath environment in the aqueous calcium bath, thus reducing the encapsulation efficiency. In this study, gallic acid was added at an isotonic level in the calcium chloride solution to keep the EE value high. Despite this, it is thought that the reason for the lower EE value is the washing process with pure water after the bead production. To prevent the beads

Research Article
doi.org/10.1002/slct.202404272

Chemistry Europe
European Chemical Societies Publishing

Table 5. Final equation in terms of actual factors.

Variables	EE	PY	LC	PD	AR	Circularity	Sphericity	(PDI)^1/2	D10	D50	D90	Span
Intercept	74.30	290.11	9.28	3.39	1.23	0.12	74.31	0.35	3.13	3.54	3.82	1.47
X_1	56.88	37.64	2.29	0.47	−1.17	0.25	32.37	−0.05	0.49	0.46	0.51	−0.21
X_2	9.36	–	−2.69	0.74	0.06	−0.07	−8.43	−1.75	1.00	1.02	0.87	−8.57
X_3	−0.36	−0.74	−0.02	−0.01	0.0001	0.001	0.01	0.001	−0.01	−0.01	−0.01	0.01
X_4	0.65	1.98	0.02	0.03	0.04	−0.004	−0.87	–	0.03	0.03	0.03	–
X_5	−2.51	1.39	−0.23	−0.09	−0.03	–	–	–	0.02	0.02	−0.04	–
X_1X_3	–	–	–	–	0.0002	-4.00×10^{-5}	−0.003	–	–	–	–	0.0001
X_1X_4	0.33	−0.60	−0.02	−0.01	−0.01	0.002	0.34	—	−0.01	−0.01	−0.01	–
X_2X_3	–	–	–	−0.001	–	–	–	–	−0.001	−0.001	−0.001	–
X_2X_4	–	–	0.07	–	–	–	–	–	–	–	–	–
X_2X_5	–	–	–	0.07	0.05	–	–	–	–	–	0.09	–
X_3X_4	–	–	–	–	-1.10×10^{-5}	–	–	–	–	–	–	–
X_1^2	−0.19	–	−0.38	–	0.33	−0.05	−9.03	–	–	–	–	–
X_2^2	–	–	–	–	–	–	–	1.33	–	–	–	6.43
X_3^2	−7.78	0.0005	9.99×10^{-6}	7.91×10^{-6}	–	-8.85×10^{-7}	–	-7.62×10^{-7}	8.18×10^{-6}	8.68×10^{-6}	9.14×10^{-6}	-3.75×10^{-6}
X_5^2	0.0002	–	0.03	0.01	–	–	–	–	–	–	–	–
Standard error deviation	3.57	9.40	0.2338	0.0826	0.0507	0.0172	1.77	0.0219	0.0920	0.0924	0.0932	0.0540
Coefficient of variation (%)	9.72	6.80	4.25	9.04	3.63	2.13	2.07	23.69	11.21	10.22	9.16	22.46
R-squared	0.9586	0.7913	0.8458	0.9427	0.9843	0.9764	0.9745	0.8124	0.9201	0.9205	0.9327	0.8534
Adjusted R^2	0.9399	0.7343	0.7647	0.9126	0.9756	0.9674	0.9656	0.7733	0.8896	0.8902	0.9024	0.8115
Predicted R^2	0.9055	0.6382	0.6253	0.8547	0.9531	0.9505	0.9456	0.7021	0.8338	0.8347	0.8430	0.7571
Adequate precision	22.96	14.04	15.20	20.13	38.22	30.19	33.39	13.30	17.72	18.18	21.83	14.50

X_1: Alginate concentration, X_2: nozzle diameter, X_3: frequency, X_4: distance, X_5: flow rate.

Research Article
doi.org/10.1002/slct.202404272

Chemistry Europe
European Chemical Societies Publishing

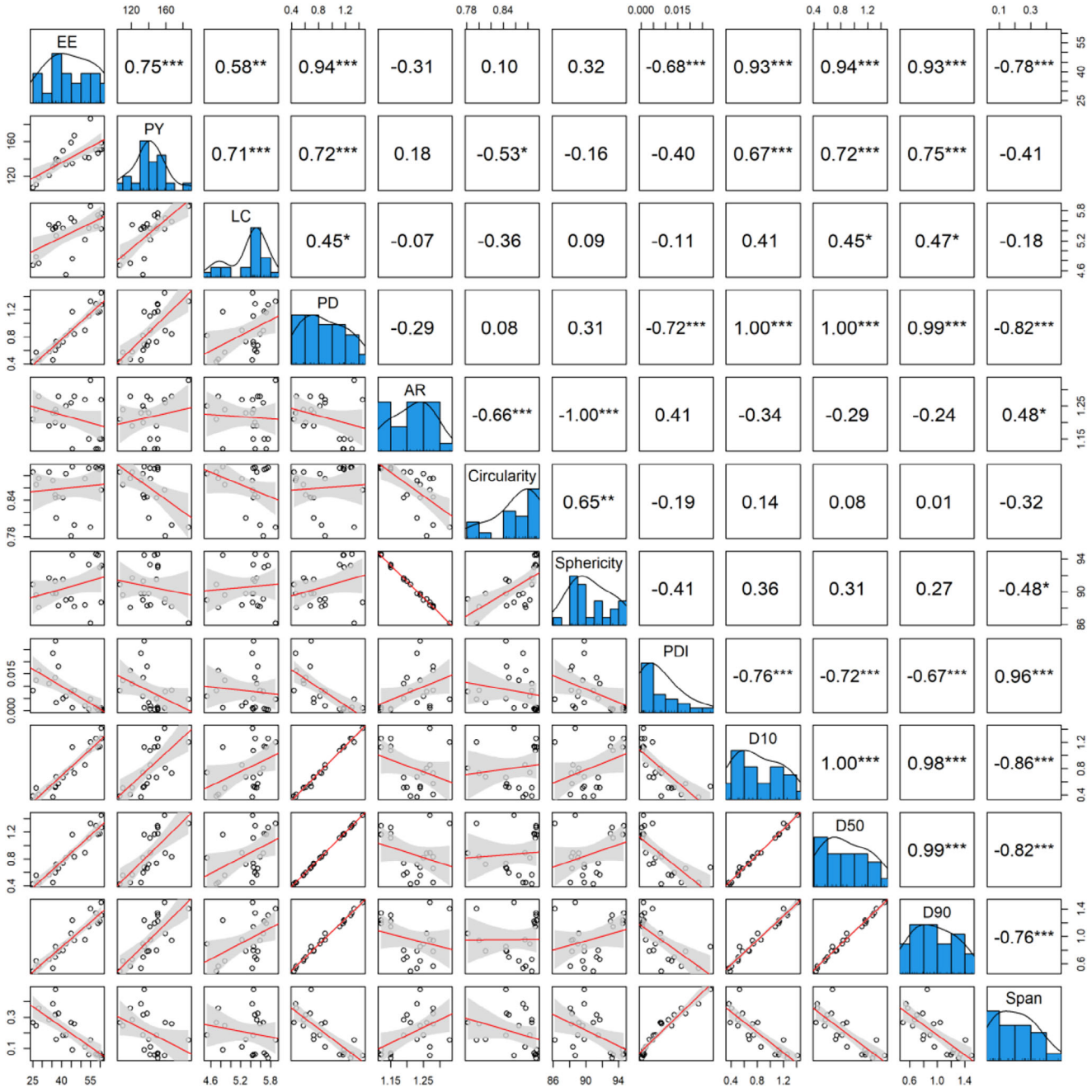

Figure 3. Correlation values between all responses.

from sticking to each other, an isotonic preparation of the washing solution used in the washing process of calcium chloride could have prevented this. Although alginate is among the most commonly used materials for the encapsulation of various active compounds in foods, it has been reported that encapsulation of gallic acid in calcium alginate beads results in low encapsulation efficiency.[3] A study on gallic acid-loaded calcium alginate beads reported an average of 20% encapsulation efficiency.[4] In an optimization research of gallic acid encapsulation in calcium alginate beads, a maximum of 42.8% for the encapsulation efficiency was achieved.[3] In our technique, it was possible to reach EE values over 50% (with a maximum of 60.7%), and the results were significantly higher than the EE values reported in the literature.[3,4]

On the other hand, the EE of the alginate beads, along with the particle stability and structural integrity, is critically influenced by the nature and concentration of the cross-linker. Ionic cross-linkers, such as calcium chloride ($CaCl_2$) and barium chloride ($BaCl_2$), serve as the most common agents by inducing the gelation of sodium alginate via the formation of "egg-box" junctions. In these systems, the concentration and type of the cross-linker directly affect the network density of the gel, thereby modulating the pore size and permeability, which in turn dictates the extent to which the active compound is retained within

the beads.[45–47] A sufficiently high concentration of cross-linker is often correlated with an increased cross-link density, reducing the likelihood of premature leakage of the actives and thereby improving the EE. However, it is equally important to optimize these parameters because an overly dense network might restrict not only the loading capacity but also the subsequent release kinetics of the encapsulated compound.[45,47]

Crosslinkers like calcium chloride ($CaCl_2$) establish ionic connections between the divalent calcium ions and the negatively charged carboxyl groups of alginate, leading to the development of a 3D gel network. This work employed calcium chloride as a crosslinking agent to facilitate the gelation of the alginate matrix. The strong affinity of Ca^{2+} ions for the guluronic acid blocks in alginate facilitates the creation of robust and stable hydrogel beads, thus improving the trapping of the core material and reducing the diffusion-related losses during and after encapsulation. Calcium chloride functions as a gelling agent and enhances the encapsulation efficiency in this technique.

3.3. Production Yield (PY)

The PY results varied between 86.40% and 186.40% (Table 3). As seen in Table 4, the alginate concentration, frequency, distance, flow rate, and alginate concentration/distance interaction were effective on PY. The frequency value stands out as the parameter that affects PY most ($p < 0.001$). The reduced quadratic model R^2, adjusted R^2, and predicted R^2 values for PY were found to be 0.7913, 0.7343, and 0.6382, respectively (Table 5). Thus, 63.82% of the EE value can be explained with the reduced quadratic model specified in the table. The predicted R^2 value was observed to be low compared to other dependent variables. A high correlation ($r = 0.8978$) was found between the predicted and actual PY values. A slight increase in the PY value was observed with the increase in the distance value. It was determined that the PY value decreased to 750 rpm frequency values and increased again with the increase in frequency. The highest PY value was reached at the 500 rpm frequency (Figure 4). When the correlation table between the dependent variables was examined (Figure 3), positive correlations, such as 0.75, 0.72, and 0.71, were found between the PY value and the EE, PD, and LC values, respectively. Since the PY value is a variable related to the bead core material, such as EE and LC, it was found to have a higher correlation value with these two variables than other responses.

3.4. Loading Capacity (LC)

The LC results of the beads were found to vary between 4.52% and 6.90% (Table 3). As seen in Table 4, the alginate concentration, frequency, distance, flow rate, alginate concentration/distance interaction, and nozzle diameter/frequency interaction were effective on the LC. Alginate concentration, frequency, and distance are the three parameters affecting the LC most ($p < 0.001$). The reduced quadratic model R^2, adjusted R^2, and predicted R^2 values for LC were found to be 0.8458, 0.7647, and 0.6253, respectively (Table 5). Thus, 62.53% of the LC value can be explained with the reduced quadratic model specified in the table. The predicted R^2 value was observed to be low compared to other dependent variables. A high correlation ($r = 0.9251$) was found between the predicted and actual values for LC. It was observed that the LC value decreased with the increase in the alginate concentration. It was determined that the LC value decreased at 750 rpm frequency values and increased again with the increase in frequency. It is seen that the PY and EE variables have the highest correlation with the LC value, with values of 0.71 and 0.58, respectively (Figure 3).

3.5. Particle Size

While the PD results ranged from 0.43 to 1.55 mm, the alginate concentration, frequency, distance, flow rate, alginate concentration/distance interaction, and nozzle diameter/frequency interaction were effective on PD (Tables 3 and 4). Alginate concentration and frequency are the parameters with the most significant effect on PD ($p < 0.001$). The reduced quadratic model R^2, adjusted R^2, and predicted R^2 values for PD were found to be 0.9427, 0.9126, and 0.8547, respectively (Table 5), and 85.47% of the PD value can be explained by the reduced quadratic model. The correlation ($r = 0.9775$) between the predicted and actual PD values was relatively high. It was observed that the PD value increased with the increase in alginate concentration. It was determined that the PD value decreased to 750 rpm frequency values and increased again with the increase in frequency. When the correlation table between the dependent variables was examined (Figure 3), a high positive correlation of 1.00, 1.00, 0.99, and 0.94 was found between the PD value and the D10, D50, D90, and EE values. Small encapsulation sizes are essential in many industries, especially food and medicine.[48,49] In this study, the volume of the beads was reduced by approximately 67.35% with the designed magnetic dripping device. With the rotation of the magnet in the center of the magnetic system, repulsion and pull forces occur between the magnet connected to the nozzle. With the effect of these forces, the nozzle oscillates and creates a whip effect, allowing the surface tension to break early. Thus, the smaller drop sizes allow for smaller bead formation. Dorati et al. (2013) reported that the vibration applied to the nozzle reduces the particle size in a study they conducted using the Encapsulator B-395 Pro BÜCHI device.[50]

3.6. Particle Shape Analyses

While the AR results varied in the range of 1.12–2.30, the alginate concentration, nozzle diameter, frequency, distance, alginate concentration/frequency interaction, alginate concentration/distance interaction, and frequency/distance interaction affected the AR. Alginate concentration, distance, and alginate/distance interaction were the parameters with the most significant AR effect ($p < 0.001$). The reduced quadratic model R^2, adjusted R^2, and predicted R^2 values for AR were 0.9843, 0.9756, and 0.9531, respectively (Table 5), and the reduced quadratic model can explain 95.31% of the AR value. The AR variable had

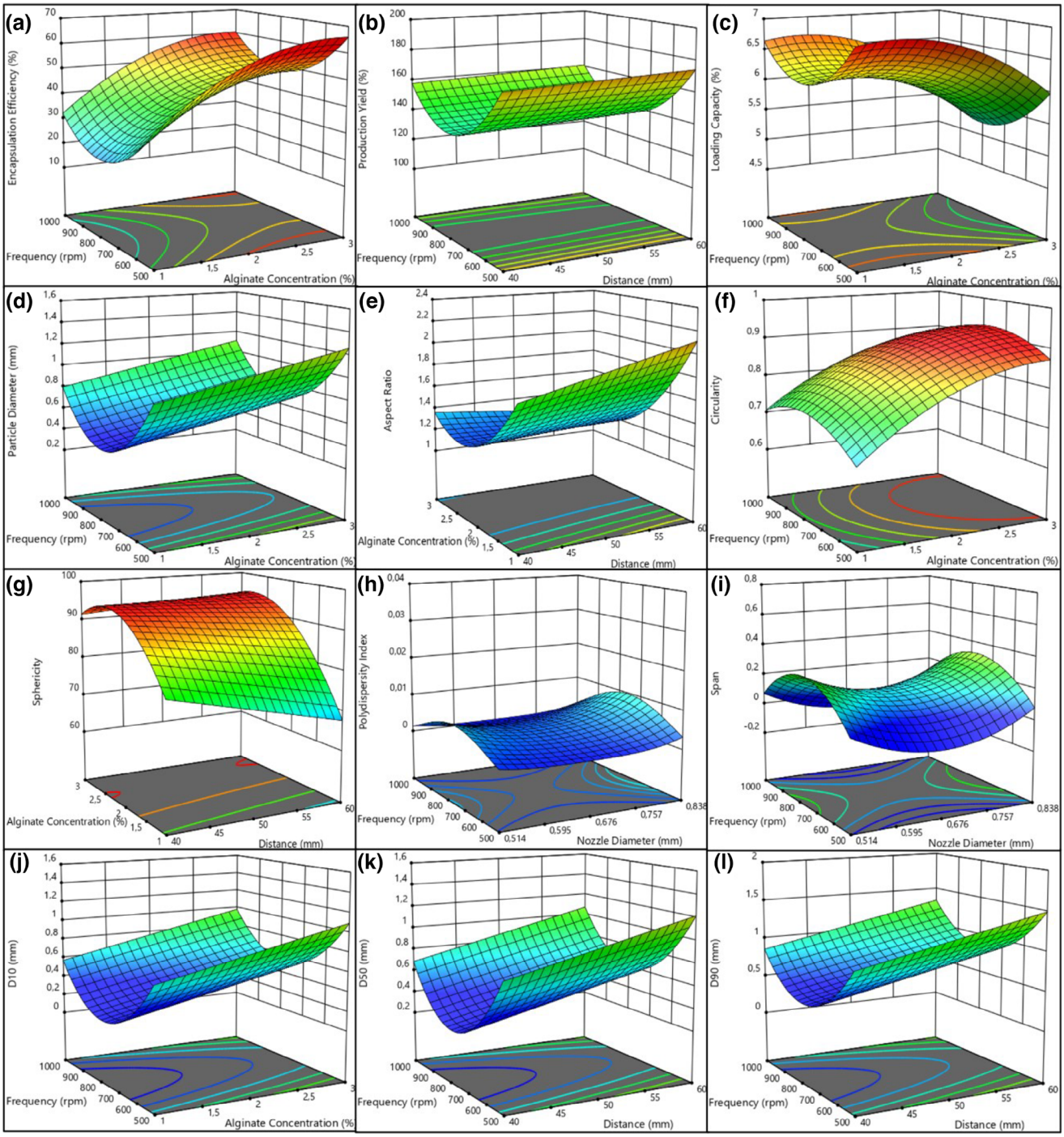

Figure 4. Three-dimensional (3D) graphs of all responses with the most effective parameters. (A) Encapsulation efficiency, (B) production yield, (C) loading capacity, (D) particle diameter, (E) aspect ratio, (F) circularity, (G) sphericity, (H) polydispersity index, (I) span, (J) D10, (K) D50, and (L) D90 values.

the highest predicted R^2 value among all responses. The correlation between the predicted and actual AR values is $R^2 = 0.9927$. Increasing the alginate concentration decreases the AR value, while increasing the distance increases it (Figure 4). Negative correlations were found between the AR value and the sphericity ($r = -1.00$) and circularity ($r = -0.66$) values (Figure 3).

It was determined that the circularity results ranged between 0.61 and 0.89 (Table 3). For a perfect circle, this value is expressed as 1.0. It was qualified that alginate concentration, nozzle diameter, frequency, distance, alginate concentration/frequency interaction, and alginate concentration/distance interaction were effective on circularity. Alginate concentration and frequency are the two parameters that significantly affect the circularity ($p < 0.001$). The reduced quadratic model R^2, adjusted R^2, and predicted R^2 values for circularity were found to be 0.9764, 0.9674, and 0.9505, respectively (Table 5). The reduced quadratic model could explain 95.05% of the circularity value. A high correlation ($r = 0.9885$) was found between the predicted and

actual values for circularity. It was observed that the circularity value increased with the increase in the alginate concentration. It was determined that the circularity value increased up to the frequency value of 800 rpm and started to decrease as the frequency increased further (Figure 4). While a statistically significant correlation was found between the circularity value and the similar terms AR and sphericity value, no high correlation was found between the other parameters. Ca^{+2} and Ba^{+2} ions are widely used in the gelation bath for cross-linking and encapsulation. However, some studies have stated that beads cross-linked with calcium might have negative features, such as not showing a smooth morphology and weak shell formation.[51] The inability of Ca^{+2} ions to provide sufficient matrix hardness at low alginate concentrations could be explained as the reason for the low circularity result at these alginate concentrations.

The sphericity values of the beads extended from 61.60 to 94.60, which was expressed as 100 for the perfect spherical structure (Table 3). It has been revealed that the alginate concentration, nozzle diameter, distance, and alginate concentration/distance interaction influence sphericity. Contrary to other dependent variables, the sphericity value was determined as the only variable in which the frequency was not statistically significant. Alginate concentration, distance, and alginate concentration/distance interaction are the three parameters that affect sphericity most ($p < 0.001$). While the reduced quadratic model R^2, corrected R^2, and predicted R^2 values for sphericity were found to be 0.9745, 0.9656, and 0.9456, respectively (Table 5), 94.56% of the sphericity value could be explained with the model. The correlation between the predicted values for sphericity and the actual values is $r = 0.9884$. As the sphericity value increases with increasing alginate concentration, it decreases with increasing distance.

In our study, it was observed that decreasing the concentration of sodium alginate led to a significant deviation from the spherical bead morphology. This behavior can be attributed to the insufficient number of carboxyl groups available for ionic interaction with the calcium ions, which are essential for the formation of a stable and uniform gel network. A similar observation was reported by Wani and Uppaluri (2023), who noted that low alginate concentrations fail to produce well-formed spherical beads due to the inadequate density of carboxyl groups required for effective crosslinking.[40] The deviation from the spherical morphology at lower alginate concentrations is consistent with the findings by Borah et al. (2024), who emphasized the significant impact of alginate content on particle shape and integrity.[41]

When Table 3 was examined, it was determined that the PDI results varied between 0.0003 and 0.0333. As the PDI value approaches zero, the degree of equidimensionality of the particles increases. As seen in Table 4, the alginate concentration, nozzle diameter, and frequency parameters were effective on PDI. Alginate concentration and frequency were determined as the two parameters with the most significant effect on PDI ($p < 0.001$). The reduced quadratic model R^2, adjusted R^2, and predicted R^2 values for PDI were found to be 0.8124, 0.7733, and 0.7021, respectively (Table 5). Thus, 70.21% of the PDI value could be explained with the reduced quadratic model specified in the table. A high correlation ($r = 0.9099$) was found between the predicted and actual PDI values. A 3D graph showing the effect of the frequency and nozzle diameter parameters on the PDI is given in Figure 4. It was determined that the PDI value increased at low and high nozzle diameters up to 750 rpm frequency values and decreased again with the increase in frequency. In the middle nozzle diameter (0.676 mm), the frequency value did not have a specific effect on the PDI. It was determined that the low and high nozzle diameters have a higher PDI value at 750 rpm than the middle nozzle diameter. The correlation between the PDI value and the spread, D10, D50, and PD values were calculated as 0.96, −0.76, −0.72, and −0.72, respectively, by analyzing the correlation table between the dependent variables (Figure 3). Since PDI is related to the span, its correlation with similar responses was higher than other parameters. Equidimensionality is one of the critical quality parameters in bead production. Because the PDI value of all beads produced in this study was lower than 0.1, the beads could be considered monodisperse.[32]

When Table 3 was examined, it was determined that the D10 values of the beads ranged between 0.37 and 1.42 mm, the D50 values between 0.43 and 1.50 mm, and the D90 values between 0.50 and 1.87 mm. It was determined that the alginate concentration, frequency, distance, flow rate, and alginate concentration/distance interaction were effective on the D10 and D50 values. It was observed that the nozzle diameter, frequency, distance, flow rate, alginate concentration/distance interaction, nozzle diameter/frequency interaction, and nozzle diameter/flow rate interaction were effective on the D90. Alginate concentration, frequency, and distance are the three parameters that have the most effect on the D10 and D50 values, while frequency, distance, and alginate/distance interaction stand out as the three parameters with the most influence on the D90 value ($p < 0.001$). For the D10 value, the reduced quadratic model R^2, adjusted R^2, and predicted R^2 values were 0.9201, 0.8896, and 0.8338, respectively. These values were 0.9205, 0.8902, and 0.8347 in D50 and 0.9327, 0.9024, and 0.8430 in D90, respectively (Table 5). Thus, 83.38%, 83.47%, and 84.30% of the D10, D50, and D90 values could be explained with the reduced quadratic model. The correlation between the predicted and actual values for D10, D50, and D90 was determined as 0.9686, 0.9686, and 0.9730, respectively. Three-dimensional graphics showing the parameters affecting the D10, D50, and D90 values are shown in Figure 4. It was observed that the D10 value increased with increasing alginate concentration, and the D50 and D90 values increased with increasing distance. It was established that the D10, D50, and D90 values decreased to 750 rpm frequency values and increased again with the increase in frequency. In addition, very high correlations were found between the D10, D50, D90, EE, PD, and span values (Figure 3).

The span values provide information about the size distribution of the particles, such as the polydispersity index. When Table 3 was examined, it was determined that the span results varied in the range of 0.04–0.48. As the span value approaches zero, the degree of equidimensionality of the particles increases. As seen in Table 4, the alginate concentration, nozzle diameter, frequency, and alginate/frequency interaction parameters were effective on the span. Alginate concentration, nozzle

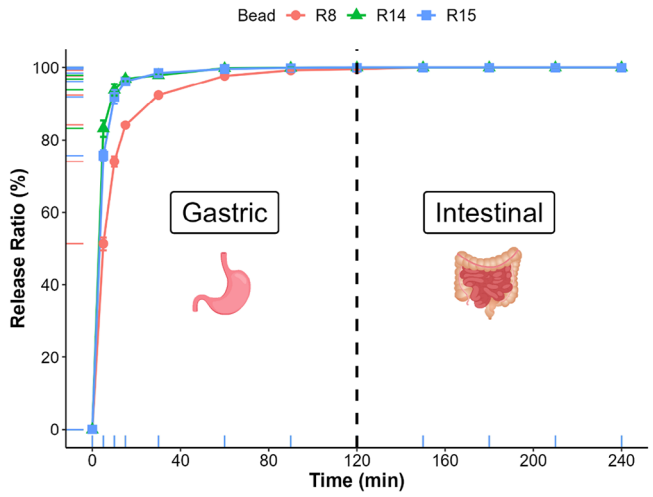

Figure 5. In vitro gastrointestinal gallic acid release profiles of the selected beads.

diameter, and frequency are the three parameters that influence it most (p <0.001). The reduced quadratic model R^2 corrected R^2, and predicted R^2 values for span were 0.8534, 0.8115, and 0.7571, respectively (Table 5), and 75.71% of the span value could be explained with this model. A high correlation (r = 0.9322) was found between the predicted and actual values. It was determined that the span value increased to 750 rpm frequency values and decreased again with the increase in frequency. At around 750 rpm, the nozzle reaches its maximum amplitude. During this amplitude, the droplet sizes decrease, but the uniform droplet formation decreases. Therefore, the PDI and span values increase at these frequency values, and the equidimensionality decreases. It was determined that the span value decreased to 0.676 mm nozzle diameter and increased again with the increase of the nozzle diameter. Hosseini et al. (2013) found the span factor values of the beads obtained by using the emulsion technique to be 0.44–0.69 in their study.[33] This study revealed that the equidimensionality of the beads produced according to the ionic gelation principle with the magnetic system is at higher levels than the emulsion method. Vibration technology is combined with the extrusion method to prevent non-homogeneous particle formation (in classical extrusion techniques).[21]

3.7. In Vitro Release Kinetics

For the beads produced in this study, high release rates were obtained using a core material with very high water solubility (i.e., gallic acid). The gallic acid release profiles of the selected beads are shown in Figure 5. After gastric digestion, the selected beads released almost all the gallic acid they contained. This indicates the inability of the calcium alginate beads alone to provide sufficient protection of the core material in acidic conditions. Gholamian et al. (2021) also reported a high release (96.02%) of cumin essential oil from alginate beads in simulated gastric fluid due to degradation and erosion processes.[43] Similar findings were noted by López Córdoba et al. (2013) and Anbinder et al. (2011), who attributed the release to the structural instability of calcium alginate in acidic media.[52,53] Furthermore, earlier research confirmed the inefficiency of calcium alginate hydrogels in preventing release under simulated gastric conditions (Almeida & Almeida, 2004; Østberg et al., 1993).

Our previous study showed that the encapsulation efficiency decreased in ionic gelation with increasing water solubility of the core material.[24] This is due to the transition of the water-soluble core material from the porous structure of the alginate–calcium bead to the aqueous medium. An additional wall material can be added to the formulation as a filling material in order to reduce the release rate and prolong the release time in the core material beads with high water solubility.

The gallic acid release data of the selected beads were fitted with the exponential (Equation 6) and hyperbolic (Equation 7) equations. The model parameters with standard errors and the statistical criteria (adjusted determination coefficient (adjusted R^2) and root mean square error (RMSE) values were given in Table 6. Both equations showed relatively high adjusted R^2 and low RMSE values. The higher b values in the exponential equations and the lower b values in the hyperbolic equations indicate higher release rates. R8 beads had lower release rates for both equations, followed by R15 and R14. In the release analyses, the size and shape of the beads affect the release rate, as they determine the surface area of the beads and the distance required for the diffusion of the core material.

4. Conclusion

Within the scope of this study, an encapsulator device system was designed using the magnetic field principle and produced as a prototype. After installing the device system, the important parameters and operating ranges were determined by preliminary experiments. Accordingly, five different parameters were studied: alginate concentration (1–3% w/v), nozzle diameter (0.514–0.838 mm), frequency (500–1000 rpm), distance (40–60 mm), and flow rate (1.0–8.0 mL/min). The effects of these parameters on bead properties such as EE, PY, LC, PD, AR, circularity, sphericity, PDI, span, D10, D50, and D90 were investigated using RSM-CCD. With the rotation of the magnet in the center of the magnetic system, repulsion and pull forces occur between the magnet connected to the nozzle. With the effect of these forces, the nozzle oscillates and creates a whip effect, allowing the surface tension to break early. Thus, the smaller drop sizes allow for smaller bead formation. In addition, the production rate increased significantly (up to five times). In the ionic gelation method, increasing the flow rate affects the production rate and particle size, but if the flow rate is increased too much, dripping turns into regular flow, ending up with aggregation. The designed magnetic system creates oscillation, which helps to overcome this problem. With this system, it was possible to reduce the bead size and to increase the production capacity and the encapsulation efficiency of gallic acid encapsulated in the calcium alginate beads. Our results showed that the proposed magnetic pulse encapsulator design is a promising system for the encapsulation and controlled release of gallic acid and

Table 6. Parameters ± standard errors of the fits of the exponential (Equation 6) and hyperbolic (Equation 7) equations of in vitro gallic acid release together with adjusted determination coefficient (adjusted R^2) and root mean square error (RMSE) values.

	Model Values	Beads		
		R8	R14	R15
Exponential	a	99.18 ± 0.36	99.49 ± 0.23	99.63 ± 0.18
	b	0.136 ± 0.003	0.349 ± 0.010	0.276 ± 0.005
	Adjusted R^2	0.9956	0.9976	0.9986
	RMSE	1.7603	1.1984	0.9244
Hyperbolic	a	103.00 ± 0.46	100.83 ± 0.22	101.37 ± 0.38
	b	4.193 ± 0.167	0.934 ± 0.046	1.390 ± 0.087
	Adjusted R^2	0.9950	0.9984	0.9953
	RMSE	1.8634	0.9912	1.6900

can be used for further applications of water-soluble phenolic compounds.

In addition, the designed system could be adapted to the multiple nozzle system (could be fed from a single source using a manifold/collector or from different sources); production with higher capacity, simultaneous production of beads with different characteristics, and pilot/industry-scale production would be possible. This scalability improves the method's practical usefulness across numerous sectors, including pharmaceuticals, nutraceuticals, and functional food industries, where efficient and uniform encapsulation is essential. Future research may concentrate on further optimizing the magnetic encapsulation system by augmenting the number of nozzle tips to enhance the production capacity. Investigating the scalability of this technology for industrial applications would be essential for enhancing its practical implementation in large-scale manufacturing. Furthermore, examining the integration of numerous bioactive substances and evaluating the system's efficacy under differing environmental conditions may yield significant insights for broadening its uses across other industries.

Acknowledgments

This study was financially supported by The Scientific and Technological Research Council of Türkiye (TÜBİTAK), Project No: 221O549. The authors would like to thank Bursa Technical University and Erciyes University for their infrastructure support throughout this study. The authors also acknowledge the support of TÜBİTAK for the Process Analysis and Optimization Scientific Training Program (2237-A, Project No. 1129B372201396). Special thanks are extended to the coordinators and instructors of the program for their valuable contributions to the training and scientific development.

Conflict of Interests

The authors declare no conflict of interest.

Data Availability Statement

The data that support the findings of this study are available upon reasonable request from the corresponding author. The data are not publicly available due to privacy or ethical restrictions.

Keywords: Calcium alginate beads · Gallic acid encapsulation · Magnetic pulse encapsulator · Response surface methodology

[1] C. G. da Rosa, C. D. Borges, R. C. Zambiazi, M. R. Nunes, E. V. Benvenutti, S. R. da Luz, R. F. D'avila, J. K. Rutz, *Ind. Crops Prod.* **2013**, *46*, 138–146.
[2] A. de Cristo Soares Alves, R. M. Mainardes, N. M. Khalil, *Mater. Sci. Eng., C* **2016**, *60*, 126–134.
[3] K. Essifi, M. Lakrat, D. Berraaouan, M.-L. Fauconnier, A. El Bachiri, A. Tahani, *Polym. Bull.* **2021**, *78*, 5789–5814.
[4] J. Li, S. Y. Kim, X. Chen, H. J. Park, *LWT –Food Sci. Technol.* **2016**, *68*, 667–673.
[5] E. Mitsou, V. Pletsa, G. T. Sotiroudis, P. Panine, M. Zoumpanioti, A. Xenakis, *Colloids Surf., B* **2020**, *190*, 110974.
[6] K. G. H. Desai, H. Jin Park, *Drying Technol.* **2005**, *23*, 1361–1394.
[7] V. Nedovic, A. Kalusevic, V. Manojlovic, S. Levic, B. Bugarski, *Procedia Food Sci.* **2011**, *1*, 1806–1815.
[8] E. Keven Silva, M. Angela, A. Meireles, *Food and Public Health* **2014**, *4*, 247–258.
[9] F. Gibbs, S. Kermasha, I. Alli, C. N. Mulligan, *Int. J. Food Sci. Nutr.* **1999**, *50*, 213–224.
[10] L. Qiu, M. Zhang, B. Adhikari, L. Chang, *Food Bioprocess Technol.* **2023**, *16*, 368–381.
[11] M. K. Mishra, *Handbook of Encapsulation and Controlled Release*, CRC press, Boca Raton, Florida **2015**.
[12] A. Nandy, E. Lee, A. Mandal, R. Saremi, S. Sharma, *J. Microencapsul.* **2020**, *37*, 205–219.
[13] R. Stojanovic, A. Belscak-Cvitanovic, V. Manojlovic, D. Komes, V. Nedovic, B. Bugarski, *J. Sci. Food Agric.* **2012**, *92*, 685–696.
[14] V. Marcillo-Parra, D. S. Tupuna-Yerovi, Z. González, J. Ruales, *Trends Food Sci. Technol.* **2021**, *116*, 11–23.
[15] T. Coruhli, Ph.D. Thesis, İstanbul Technical University (İstanbul, Türkiye) **2013**.
[16] I. Mourtzinos, C. G. Biliaderis, M. K. Krokida, in *Thermal and Nonthermal Encapsulation Methods*, 1st ed. (Ed: M. K. Krokida), CRC Press, Boca Raton, Florida **2017**, pp. 1–37.
[17] S. Castro Coelho, B. Nogueiro Estevinho, F. Rocha, *Food Chem.* **2021**, *339*, 127850.
[18] P. Robert, C. Fredes, *Molecules* **2015**, *20*, 5875–5888.
[19] N. Choudhury, M. Meghwal, K. Das, *Food Front.* **2021**, *2*, 426–442.
[20] C. Chen, X. Wang, W. Chen, L. Wang, *Food Bioprocess Technol.* **2024**, *17*, 544–553.

[21] M. Fangmeier, D. N. Lehn, M. J. Maciel, C. F. Volken de Souza, *Food Bioprocess Technol.* **2019**, *12*, 1472–1486.
[22] L. E. Kurozawa, M. D. Hubinger, *Curr. Opin. Food Sci.* **2017**, *15*, 50–55.
[23] S. C. S. R. de Moura, C. L. Berling, S. P. M. Germer, I. D. Alvim, M. D. Hubinger, *Food Chem.* **2018**, *241*, 317–327.
[24] H. Demircan, R. A. Oral, *Int. J. Biol. Macromol.* **2023**, *236*, 124011.
[25] C. Jeong, S. Kim, C. Lee, S. Cho, S.-B. Kim, *Foods* **2020**, *9*, 180.
[26] S. N. Jayasinghe, *J. Microencapsul.* **2007**, *24*, 430–444.
[27] L. Zhang, J. Huang, T. Si, R. X. Xu, *Expert Rev. Med. Devices* **2012**, *9*, 595–612.
[28] Y. Song, Y. K. Chan, Q. Ma, Z. Liu, H. C. Shum, *ACS Appl. Mater. Interfaces* **2015**, *7*, 13925–13933.
[29] N. E. Rahmani-Manglano, E. M. Guadix, C. Jacobsen, P. J. García-Moreno, *Antioxidants* **2023**, *12*, 266.
[30] F. Davarcı, D. Turan, B. Ozcelik, D. Poncelet, *Food Hydrocoll.* **2017**, *62*, 119–127.
[31] A. H. Morales, F. C. Spuches, J. S. Hero, A. F. Alanís, M. A. Martínez, C. M. Romero, *Food Hydrocoll.* **2021**, *117*, 106706.
[32] H. Cetin Babaoglu, A. Bayrak, N. Ozdemir, N. Ozgun, *J. Food Process. Preserv.* **2017**, *41*, e13202.
[33] S. M. Hosseini, H. Hosseini, M. A. Mohammadifar, A. M. Mortazavian, A. Mohammadi, K. Khosravi-Darani, S. Shojaee-Aliabadi, S. Dehghan, R. Khaksar, *Int. J. Biol. Macromol.* **2013**, *62*, 582–588.
[34] H. Demircan, M.S. Thesis, Bursa Technical University (Bursa, Türkiye) **2018**.
[35] P. Kiaei Pour, I. Alemzadeh, A. S. Vaziri, A. Beiroti, *J. Food Sci. Technol.* **2020**, *57*, 3363–3370.
[36] A. S. Vaziri, I. Alemzadeh, M. Vossoughi, *Food Biosci.* **2019**, *32*, 100460.
[37] B. Karaca, S. Buzrul, A. C. Cihan, *Food Sci. Animal Resources* **2021**, *41*, 288–299.
[38] M. J. Delgado-González, M. D. García-Moreno, D. A. Guillén-Sánchez, *Foods* **2022**, *11*, 517.
[39] C. A. Hoesli, K. Raghuram, R. L. J. Kiang, D. Mocinecová, X. Hu, J. D. Johnson, I. Lacík, T. J. Kieffer, J. M. Piret, *Biotechnol. Bioeng.* **2011**, *108*, 424–434.
[40] K. M. Wani, R. V. S. Uppaluri, *Biomass Convers. Biorefin.* **2024**, *14*, 19911–19928.
[41] S. Jyoti Borah, R. Kumar, P. Prasad Singh, V. Kumar, *ChemBioChem* **2024**, *25*, e202400567.
[42] S. Najafi-Soulari, H. Shekarchizadeh, M. Kadivar, *J. Biomater. Sci., Polym. Ed.* **2016**, *27*, 1631–1644.
[43] S. Gholamian, M. Nourani, N. Bakhshi, *Food Chem.* **2021**, *338*, 128143.
[44] S. Gouin, *Trends Food Sci. Technol.* **2004**, *15*, 330–347.
[45] A. K. Nayak, D. Pal, K. Santra, *J. Pharma.* **2013**, *2013*, 1–11.
[46] Y. Hosokawa, T. Goshima, T. Kai, S. Kobaru, Y. Ohzuno, S. Nii, S. Kiyoyama, M. Yoshida, T. Takei, *Materials* **2024**, *17*, 6027.
[47] K. Benfattoum, N. Haddadine, K. Beyaz, N. Bouslah, A. Benaboura, P. Maincent, R. Barillé, A. Sapin-Minet, *Adv. Pharma. J.* **2018**, *3*, 104–117.
[48] C. M. Silva, A. J. Ribeiro, I. V. Figueiredo, A. R. Gonçalves, F. Veiga, *Int. J. Pharm.* **2006**, *311*, 1–10.
[49] P. M. Reque, A. Brandelli, *Trends Food Sci. Technol.* **2021**, *114*, 1–10.
[50] R. Dorati, I. Genta, T. Modena, B. Conti, *J. Microencapsul.* **2013**, *30*, 559–570.
[51] M. Jones, D. Walker, C. M. Ionescu, B. Kovacevic, S. R. Wagle, A. Mooranian, D. Brown, H. Al-Salami, *Ther. Deliv.* **2020**, *11*, 791–805.
[52] A. López Córdoba, L. Deladino, M. Martino, *Carbohydr. Polym.* **2013**, *95*, 315–323.
[53] P. S. Anbinder, L. Deladino, A. S. Navarro, J. I. Amalvy, M. N. Martino, *J. Encapsul. Adsorp. Sci.* **2011**, *1*, 80–87.

Manuscript received: September 6, 2024